Case Studies in Construction Materials 17 (2022) e01226

Contents lists available at ScienceDirect

Case Studies in Construction Materials

journal homepage: www.elsevier.com/locate/cscm

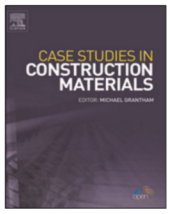

Diagnosis of ASR damage in highway pavement after 15 years of service in wet-freeze climate region

Michał A. Glinicki *, Daria Jóźwiak-Niedźwiedzka, Aneta Antolik, Kinga Dziedzic, Mariusz Dąbrowski, Karolina Bogusz

Institute of Fundamental Technological Research Polish Academy of Sciences, Pawinskiego 5b, 02-106 Warsaw, Poland

ARTICLE INFO

Keywords:
Alkali-silica reaction
Concrete
Cracking
Durability
Highway pavement

ABSTRACT

Diagnostic tests were carried out on specimens drilled from a section of jointed, unreinforced highway pavement after 15 years of service. The section of highway was exposed to heavy road traffic, environmental actions of wet-freeze climate zone and associated winter maintenance including application of deicing salt. Premature pavement damage was manifested by visible cracking, mostly along transverse joints and in slab corners. Tests performed on core specimens included petrographic analysis of concrete and its components, using optical and scanning electron microscopy, also evaluation of elastic and transport properties, expansion potential, cracks and air void system. Numerous cracks in the grains of coarse quartzite aggregate were found. Reactive forms of quartz in quartzite aggregate - microcrystalline and cryptocrystalline quartz - were abundant. The gel-like products in cracks in quartzite grains and in surrounding cement paste were identified as alkali-silica reaction products. Expansion of specimens exposed to an alkali-silica reaction-promoting environment indicated the potential for further development of such reaction. Substantial cracking and reduction of modulus of elasticity was correlated with the presence of reactive quartz in quartzite aggregate. The role of additional destructive factors, such as the impact of heavy vehicles traffic and freeze-thaw aggression was indicated by greater cracks in the slow traffic lane compared than in the emergency lane, associated with local marginal air entrainment of concrete.

1. Introduction

Diagnosing premature concrete damage in highway pavements requires careful analysis of various possible failure mechanisms. The frequent wetting of the pavement due to precipitation causes that the pavement slab is generally kept with a high degree of water saturation. The exception is the subsurface layer with a thickness of several cm, which is subject to drying out and re-wetting in accordance with weather changes. One of the reasons for damage to wet concrete in pavements may be the alkali-silica reaction (ASR), provided that reactive silica minerals are present in concrete aggregates and cement with a sufficiently high content of alkali or other sources of alkali ions are present. Damage to road and airport concrete pavements as a result of ASR was reported in few countries, [1–3]. The development of an extensive network of closely spaced cracks is one of typical symptoms of ASR in pavements [4]. Most often reported signs of ASR damage comprised of map-cracking in the vicinity of joints, joint spalling, aggregate pop-outs or extrusion

* Corresponding author.
E-mail addresses: mglinic@ippt.pan.pl (M.A. Glinicki), djozwiak@ippt.pan.pl (D. Jóźwiak-Niedźwiedzka), aantolik@ippt.pan.pl (A. Antolik), kdzie@ippt.pan.pl (K. Dziedzic), mdabrow@ippt.pan.pl (M. Dąbrowski), kgibas@ippt.pan.pl (K. Bogusz).

https://doi.org/10.1016/j.cscm.2022.e01226
Received 2 March 2022; Received in revised form 13 May 2022; Accepted 4 June 2022
Available online 8 June 2022

of joint-sealing material between adjacent sections of concrete pavement [5,6]. The signs of on-going reaction included also surface discoloration and exudation associated with cracks. Further cracking of concrete could result in developed spalling, surface popouts, major deterioration of joints. Such damage caused by the development of ASR could generate loose pieces of the pavement, known as foreign object debris, that are of special concern in airport facilities because an accidental ingestion by jet engines can cause severe aircraft damages. In case the expansion joints have closed, anisotropic restraint also develops in pavements, causing the development of aligned, parallel cracking.

The extent of problems caused by ASR in airport or highway pavements varied from exacerbated surface cracking to more severe damages that impaired the serviceability of slabs, inducing a need for reconstruction [4]. The petrographic analysis of cored specimens from pavements revealed typical signs of ASR such as cracked coarse aggregates with gel-like deposits filling the cracks. The damage-cause recognition in each of the pavement cases reported in [7–9] was fundamentally supported by the presence of alkali-silica reaction products within cracks in aggregate, within the paste-aggregate interface or inside air voids. Reactive aggregates involved in these cases covered glassy volcanic rocks, highly reactive siliceous limestone as well as natural gravel (predominantly granitic and metasedimentary) and crushed porphyritic volcanic rock, respectively. Numerous other reactive rock aggregate in pavement concrete were studied by Frybort [10], like metamorphosed volcano-sedimentary complex rocks, including proterozoic chert, black shale, spilite, and green schist, and alluvial sandy gravels. The rock type of aggregate was established as the crucial factor for occurrence of ASR as well as for the composition of its deleterious products.

The diagnostic studies of Denver airport pavement revealed the distress consisting of significant surface cracking attributed to ASR [4]. The presence of ASR in different locations, shown by typical signs such as cracked coarse aggregates with gel deposits filling the cracks, was mostly related to the reactivity of dark brown granite aggregates used. A number of deterioration mechanisms was detected, including scaling of variable severity. The service life of concrete runway was shortened to 15 years, from the expected 20–30

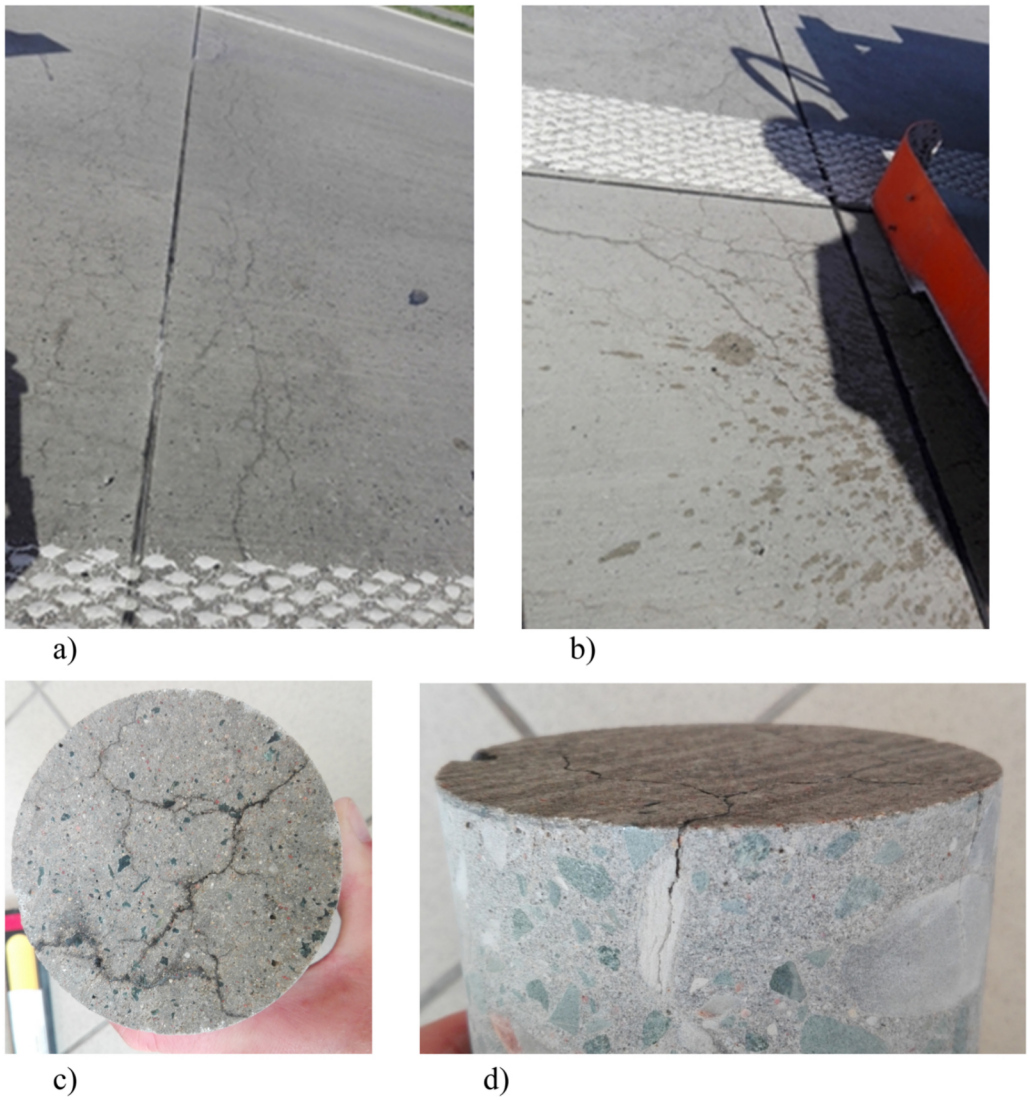

Fig. 1. Typical cracks and crack patterns observed at the surface near joints in highway pavement (a, b) and in the cores ϕ 100 mm taken from the pavement (c,d).

years, as a result of combination of deterioration mechanisms. A coupled action of freeze-thaw cycles and alkali-silica reaction is known from a field study of concrete barriers exhibiting moderate to severe deterioration and laboratory studies reported in [11,12]. Test results demonstrated that concrete deterioration with borderline-reactive aggregates could not be attributed to ASR alone, indicating the deterioration enhancement by freezing and thawing action.

No symptoms of concrete deterioration highway pavements due to alkali-silica reaction have been reported in Poland. A survey of concrete structures deteriorated due to ASR made by Góralczyk [13] revealed only few road viaducts and buildings affected. In this paper the case of busy highway pavement in wet-freeze climate zone is examined after 15 years of service. The reason for the examination was the premature pavement damage revealed by the visual survey. The objective of the paper is to evaluate whether ASR could be identified as a main cause of the observed pavement surface distress. The range of experimental work typical for ASR detection was extended to recognize possible influence of other deterioration mechanisms.

2. Experimental

2.1. Field observations, specimens and mix design data

Visual examination of highway section revealed premature signs of distress as shown in Fig. 1. There were cracks in multiple pavement slabs, visible at the surface on all three traffic lanes. The cracks were located in the vicinity of cut joints, primarily along the transverse joints or in slab corners. Due to transverse joint spalling in few slabs, the repair patches were observed too. As shown in Fig. 1, some crack patterns was observed; the maximum crack width was up to 2 mm. Dark discolorations along transverse joints were also observed at dry weather conditions, indicating an elevated water saturation in the vicinity of joints. The map crack pattern with the spacing of several centimeters was observed. The cracks seen at the surface could be traced to the depth of several cm. As shown in Fig. 1d, such cracks were seen to pass through large aggregate grains of bright beige/light grey color, but not through darker grey/greenish color aggregate. No major signs of surface scaling were noted.

The highway section is located in the central part of Poland in wet-freeze climate zone. In this area the winter season, defined as the period with average daily temperature below 0 °C, lasts about 94 days (the average established between 1981 and 2013), Accordingly, the regulations specify winter maintenance for highways [14] - the road slipperiness is reduced by de-icing chemicals, the most common being 20–25% water solution of NaCl spray applied on pavement surface at the application rate of 15–160 ml/m^2.

The core specimens of 100 mm in diameter were taken from several locations (Table 1). The core specimens were taken both from cracked slabs and uncracked ones.

Mix design data and properties of aggregate available from archived reports are presented in Tables 2 and 3. The properties of materials were in conformity with standard specifications. The properties of air-entrained concrete evaluated on test specimens cast during the construction were the following:

- the 28-days cube compressive strength from 40.1 to 60.8 MPa,
- the 28-days flexural strength from 3.9 to 6.3 MPa,
- the water absorption by mass from 3.9% to 4.6%,
- the adequate frost resistance, evaluated by the reduction of compressive strength after 150 freeze-thaw cycles from 4.0% to 13.1% (mostly <10%; specified limit <20%).

The target compressive strength of concrete 40 MPa was met, the required low water absorption and high frost resistance was provided, but some specimens failed to meet the specified flexural strength of 5.5 MPa at the age of 28 days.

Table 1
Location of core sampling on highway pavement.

Core #	Mileage, roadway, traffic lane	
	Slow-traffic lane	Emergency lane
1		339 + 200, SW bound roadway
2	338 + 870, SW bound roadway	
3		336 + 180, SW bound roadway
4		335 + 900, SW bound roadway
5	336 + 160, SW bound roadway	
6		334 + 650, NE bound roadway
7		335 + 600, NE bound roadway
8	336 + 100, NE bound roadway	
9	336 + 755, NE bound roadway	
10	337 + 170, NE bound roadway	

Table 2
Concrete mix design.

Component	Contents [kg/m^3]
Portland cement CEM I 32.5 R[a)]	360
Water	144
Natural sand 0/2 mm	551
Crushed amphibolite 2/8 mm	228
Crushed amphibolite 8/16 mm	475
Crushed quartzite 16/32 mm	645
Air entraining admixture	0.576
Water reducing admixture	1.80

[a] the alkali content not available

Table 3
Properties of aggregate.

Type of aggregate	Apparent density [g/cm^3]	Water absorption[a] [%]	Alkali-aggregate reactivity[b]	Frost resistance[c] – mass loss [%]
Natural sand 0/2 mm	2.66	n.d.	nonreactive	n.d.
Crushed amphibolite 2/8 mm	2.91	0.6	nonreactive	1.81
Crushed amphibolite 8/16 mm	2.93	0.3	nonreactive	0.32
Crushed quartzite 16/32 mm	2.70	0.5	nonreactive	0.36

[a] per [15]; the specified limit $< 1.5\%$
[b] „zero" degree of reactivity as per [16]; as specified. *The quick determination of potential alkaline reactivity of aggregate based on the mass loss of aggregate (fine or coarse) exposed to sodium hydroxide solution at 90 °C and the content of reactive flint in coarse aggregate.*
[c] mass loss as per [17]; the specified limit $< 2\%$

2.2. Test methods

The petrographic evaluation of microstructure and determination of physical properties of concrete was performed on appropriate specimens cut from the cores with a diamond saw. The most damaged pieces of concrete fell apart during cutting. Microscopic observations on polished sections or thin sections were made on vertical sections of the pavement slabs. The applied test methods are listed in Table 4.

The crack system analysis was performed on thin sections cut out of three cores from the slow-traffic lane and three cores from the emergency lane. Each section area was about 1000 mm^2. Microscopic images acquired at the magnification 40x using UV light source were subjected to digital processing using automated image analysis system Image Pro Plus 7.0. It consisted of the binarization, application of shape constraints for air void removal, further morphological transformations (dilation and erosion) to remove abnormal crack discontinuities; eventually the skeletonization transformation was applied, to enable the determination of the total (dendritic) length of cracks [23]. An extended analysis was performed on selected specimens from the slow-traffic lane and emergency lane to obtain digital reconstruction of coarse aggregate distribution and the crack system so as to allow for separation of cracks within the grains and within the matrix area (Fig. 2). Crack system analysis was also performed on virgin quartzite aggregate not used for concrete.

Table 4
Test methods applied for concrete diagnostics.

Test method	Specimens
Macroscopic evaluation of aggregate grain distribution, large voids and major cracks in the cross-section – the internal standard method based on ASTM C856[18]	flat vertical sections of cylindrical core specimens 100 mm in diameter
Thin sections examination by optical microscopy (identification of reactive minerals in aggregate grains, quantitative evaluation of reactive minerals, identification of alkali-silica reaction products) as per RILEM AAR-1[19,20], ASTM C295[21]	thin sections 26 × 38.5 mm, 20 μm thick, cut from cores within the top 50 mm layer and vacuum-impregnated with fluorescent epoxy resin
Composition identification of alkali-silica reaction products on polished sections - scanning electron microscopy with EDS microanalysis as per ASTM C1723[22]	polished sections 25 × 45 mm cut from cores (from the top layer of the core or from the mid-height)
Evaluation of crack system and microcrack system using digital analysis of optical thin section images and SEM images of polished sections,[23]	thin sections and polished sections as above, vacuum-impregnated with fluorescent epoxy resin
Elastic modulus determination using the resonant method as per ASTM C215[24]	prisms 30×25×240 mm cut from the cores
Residual expansion evaluation by expansion measurements of cut specimens exposed to accelerated alkali-silica reaction environment (1 M NaOH, 80 °C) as defined by ASTM C1260[25]	prisms 30×25×240 mm cut from cores; with embedded steel studs
Air void characteristics and rate of water absorption as per PN-EN 480–11[26] and ASTM C1585[27], respectively	polished sections 100 × 100 mm and disks ϕ100 by 50 mm thick cut from cores
Evaluation of the potential reactivity of quartzite aggregate using: a) accelerated mortar bar test as per ASTM C1260; b) miniature concrete prism test as per AASHTO T380[28]	standard specimens cast with quartzite aggregate and Portland cement

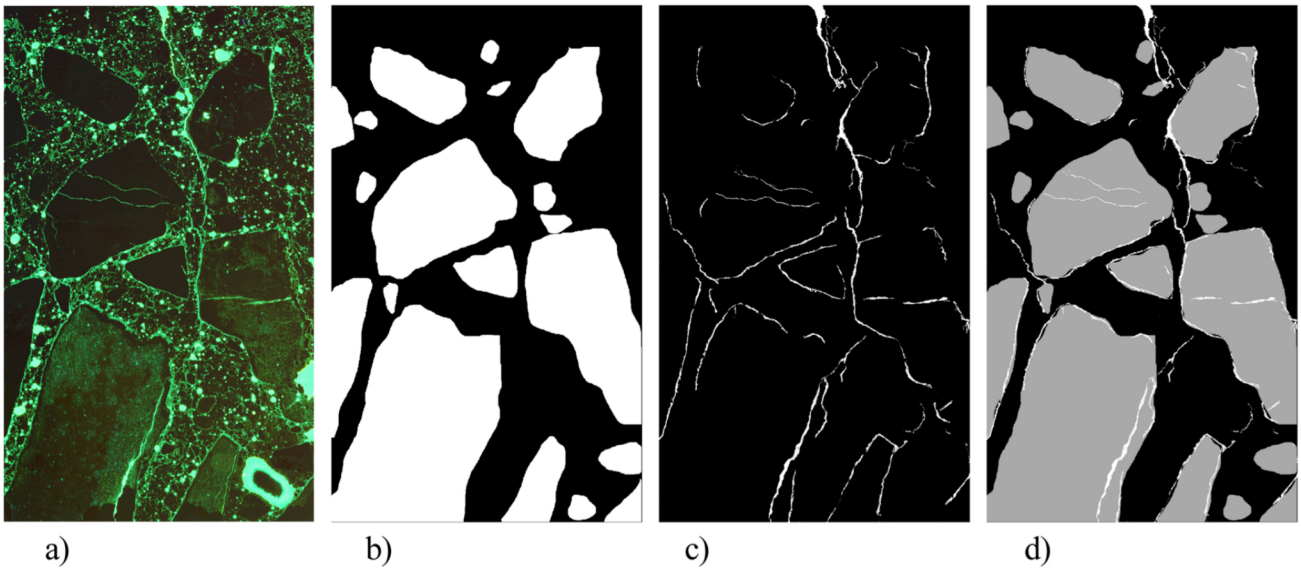

Fig. 2. Effects of morphological transformations of thin section image of concrete core specimen: a) original microscopic image under UV light, b) separated coarse aggregate grains, c) crack system after removing the matrix and non-crack-like objects, (d) combination of crack system and coarse aggregate image (the size of each image: 26 ×38.5 mm).

For the analysis of microcracking of quartzite aggregate grains, the plane impregnated polished sections of concrete cores were used as well as polished specimens containing pristine quartzite aggregate only. The scanning electron microscopy was used to acquire the images of entire surface of polished sections 25×45 mm at a magnification of 300x (only images containing quartzite grains were selected, from 200 to 280 images for each section). The images were binarized in the range (0−105) and subjected to the morphological transformations as described above. After skeletonization transformation, the nodal points were subtracted from the microcrack system image.

Supplementary tests were performed on quartzite aggregate acquired from current production of the same quarry. Evaluation of the potential reactivity of quartzite aggregate was performed on laboratory-manufactured standard specimens for accelerated mortar bar test and miniature concrete prism test. The equipment for testing and software was described elsewhere [29,30]. Non-standard technique for quartz size identification in quartzite aggregates was performed using the method described in [20]. Following the original idea of Castro and Wigum [31], it was meant as a supplementary tool to recognize the potential reactivity of aggregates.

3. Test results

3.1. Macroscopic evaluation, microscopic analysis of minerals and reaction products

The macroscopic analysis of concrete revealed a homogeneous distribution of coarse aggregate grains in the cross section. Clearly visible cracks were observed within bright aggregate grains in contrast to dark aggregate grains free of visible cracking. White gel substance was visible in cracks of aggregates and in large air voids. The content of large air voids (larger than 2 mm in diameter) was up to 1.8% and 2.8% within the upper and the lower part of pavement slab, respectively. Large cracks parallel to the road surface were noticed in the lower half of core, passing both through the matrix and coarse aggregate. Cracks in the cross-section of concrete cores were clearly visible even in the case of only minor cracking seen at the pavement surface.

The thin section observations were carried out in transmitted light with parallel polarizers (PPL), crossed polarizers (XPL), also with gypsum plate (XPL_G) and in ultraviolet light (UV). As a result of the petrographic analysis of aggregate in concrete, it was found:

- the presence of crushed quartzite rock (composed mainly of quartz, Fig. 3) and crushed amphibolite rock (composed mainly of amphibole and plagioclase) as coarse aggregate;
- the presence of quartz sand containing limestone grains as fine aggregate;
- single mudstone grains in coarse aggregate.

The medium to fine-grained quartzite is composed mainly of quartz angular particles and trace amounts of muscovite. The quartz grains shown in Fig. 3a are white to gray to black depending on their optical orientation. As shown in Fig. 3b the aggregate grains are composed of quartz crystals of various size and shape, the interlocking crystals of quartz are clearly visible. These Upper Cambrian quartzites are classified as sedimentary quartzites; they are characterized with a typical mosaic structure without cement matrix, which are composed of quartz grains with little different dimensions, isometric shapes or elongated. The quartzite is hard, dense, sometimes with small caverns and crevices partially or completely filled with quartz crystals.

The thin-sections observation revealed also the presence of gel-like substance in quartzite aggregate grains and in the surrounding

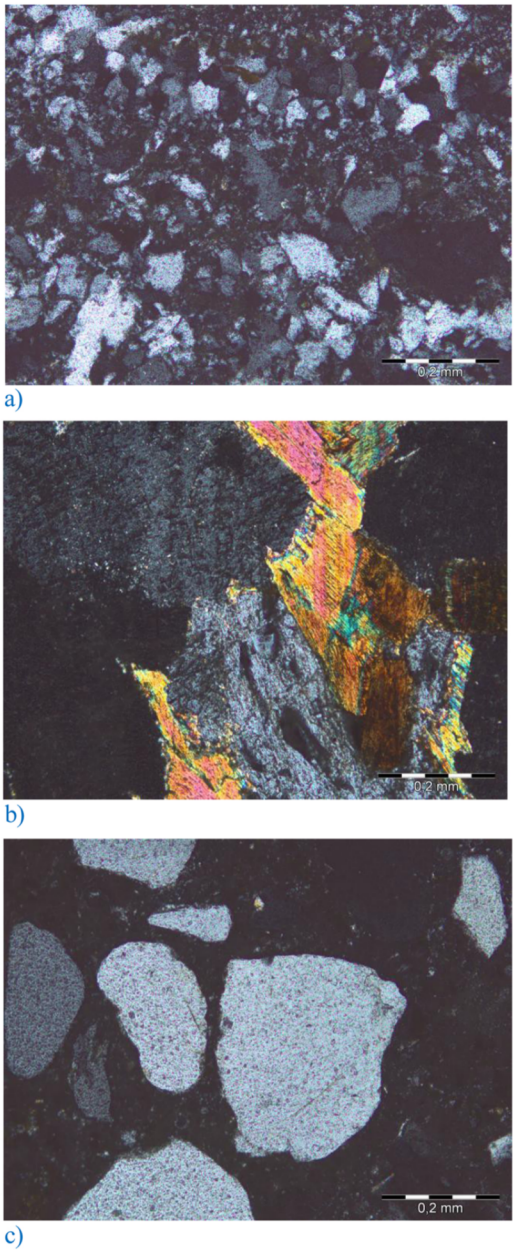

Fig. 3. Thin section in XPL aggregate in pavement concrete: a) quartzite, b) amphibolite, c) siliceous sand, scale bar 0.2 mm.

cement paste; no such products in the grains of amphibolite aggregate, nor in sand particles. Cracks and gel-like products as shown in Figs. 4 and 5. Gel-like products partially or completely filled many air voids, especially those with a diameter of up to approx. 200 μm. Some air voids were found partially filled with cement hydration products (ettringite). The abundant presence of gel-like reaction products was observed both in slow-traffic lane specimens and emergency lane specimens. The gel-like product was present in cracked quartzite aggregate; the continuity of gel filling the cracks in the aggregate and cracks in the surrounding cement paste were observed, Fig. 5.

The petrographic image analysis of aggregate grains was focused mainly on the quartz size and content. The equivalent mean diameter of separated quartz grains on the images was obtained so as to allow for grain size classification. The reactive forms of quartz are usually classified depending on the crystal size [32]. Following the terminology assumed in [33], quartz is identified as microcrystalline if < 100 μm, as cryptocrystalline if < 10 μm. The observed differences in the quartz grain size in quartzite aggregate are illustrated in Fig. 6. The presence of micro- and cryptocrystalline quartz in the grains of quartzite aggregate is abundant.

Results of digital evaluation of the content of microcrystalline and cryptocrystalline quartz in quartzite grains are given in Table 5. The estimated content of reactive forms of quartz in quartzite aggregate was large and it was found correlated with the presence of cracks in grains. The susceptibility of quartzite grains to cracking was found for the content of reactive quartz of more than 10%, while for its content of less than 7% aggregate cracking was not manifested.

Scanning electron microscopy observations confirmed the presence of gel-like products in the fractures of quartzite aggregate

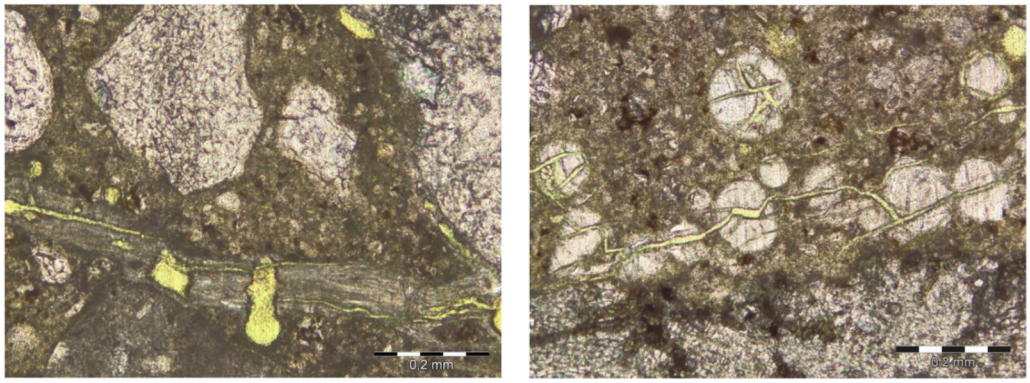

Fig. 4. Gel-like reaction products coming from quartzite aggregate, in: a) cement matrix, b) in air-voids, scale bar 0.2 mm.

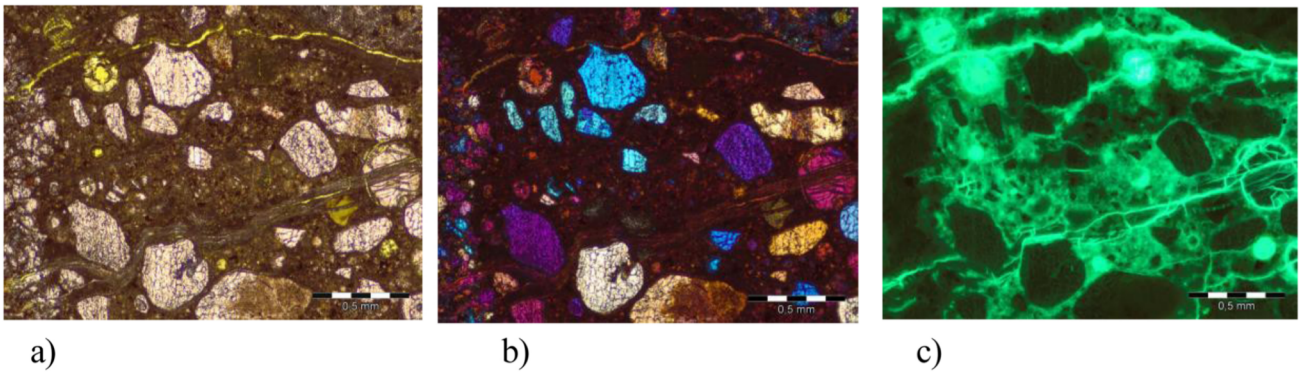

Fig. 5. Gel-like reaction product extending from quartzite grain into cement matrix and air-voids (8 A): a) PPL, b) XPL_G, c) UV; scale bar 0.5 mm.

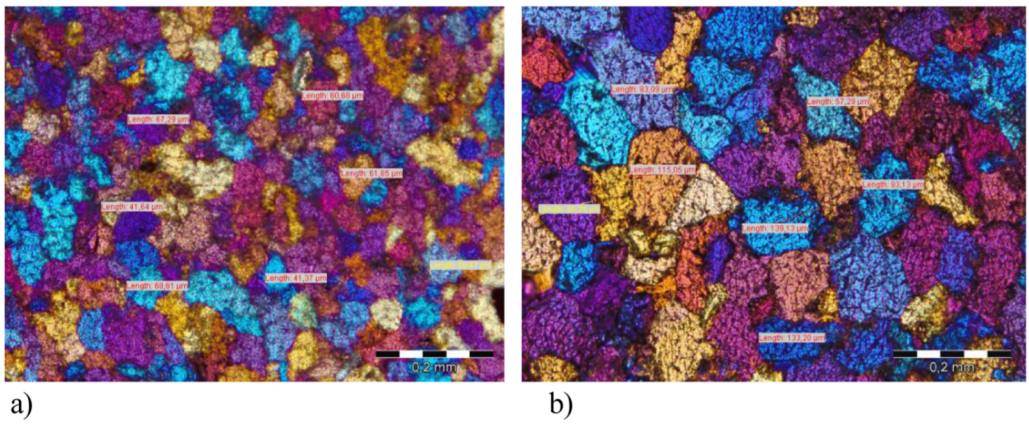

Fig. 6. Differences in the quartz grain size in quartzite: a) cracked aggregate, b) uncracked aggregate; XPL_G, (10 A), scale bar 0.2 mm.

grains, it also extended into the cement paste areas, Fig. 7. EDS microanalysis of the reaction product in micro-areas showed that it is potassium-sodium-calcium silicate with a significant atomic concentration of potassium (K), sodium (Na) and calcium (Ca), Fig. 8. The qualitative elemental composition of calcium-sodium-potassium silicate products (shown in Table 6) is found to correspond to the range of composition of alkali-silica reaction products, known from the literature. The most common atomic concentration ratio (Na + K)/Si of ASR products is about 0.2–0.35 [34–36]. The currently revealed qualitative composition of ASR products in quartzite aggregates is: (Na+K)/Si: 0.32 ± 0.09; Ca/Si: 0.57 ± 0.17.

The observed variability of ASR product composition is related to its location, either within the quartzite grain, or in cement paste or in air voids. In Fig. 9 the color maps of the concentration of elements K, Ca and Na are shown in the area of the cracked quartzite grain and in the surrounding cement paste. The color intensity change illustrates the penetration of a given ion through the grain-cement paste boundary. The concentration of Ca in ASR product increased with increasing distance from the aggregate grain

Table 5
The content of micro-and cryptocrystalline quartz in quartzite aggregate determined for cracked and uncracked grains (the average value on 8 images and the data range from-to).

Traffic lane	Thin section no.	Cross-section area of micro-and cryptocrystalline quartz in respect to total cross-section of quartzite grains [%]	
		in uncracked grains	in cracked grains
Emergency	3 A	none	14.7 (10.6–20.0)
	7 A	7.4 (4.3–9.9)	9.5 (7.9–12.1
Slow-traffic	5 A	6.4 (4.6–7.8)	22.7 (19.9–26.2)
	8 A	4.7 (3.0–6.8)	35.0 (27.9–40.0)
	10 A	5.8 (3.7–8.3)	11.0 (8.2–13.7)

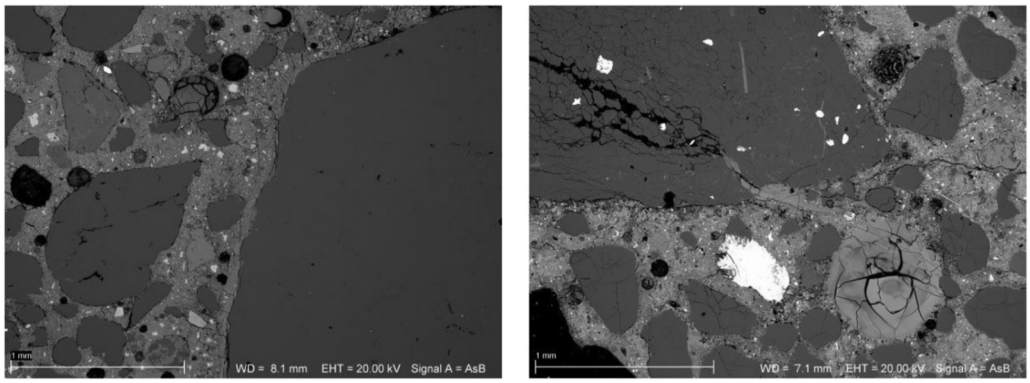

Fig. 7. ASR products in quartzite aggregate grains and in cement matrix: a) emergency lane – 7 A, b) slow-traffic lane – 8 A; scale bar 1 mm.

boundary into the paste. Such observations were reported previously [37–39]. The (Na+K)/Si ratios for ASR products in cement paste and in air voids were in average: 0.28 ± 0.11 and 0.20 ± 0.16, respectively. Observed differences in the concentration of elements in ASR products present in specimens from the slow-traffic lane and the emergency lane are not consistent and do not allow for further analysis.

3.2. Crack system evaluation

General evaluation of width of cracks observed on thin-sections of pavement concrete revealed that cracks in quartzite aggregate grains are approx. 40–80 μm wide (smaller cracks) or 250–350 μm (main crack), Fig. 10. Cracks in cement matrix filled with gel-like product were about 60 ÷ 120 μm wide. The characterization of crack system in concrete, based on digital image analysis in UV light [23] is based on the following parameters:

- the total length of cracks [mm] - sum of dendritic lengths of all detected cracks,
- the total crack area [mm^2] - sum of crack surface areas,
- the crack length ratio [mm^{-1}] – the ratio of the total length of cracks to the surface of image,
- crack surface ratio [%] – the ratio of the total area of cracks to the area of image.

The total length of the cracks per unit cross-sectional area was 0.39 ± 0.03 mm^{-1} and 0.47 ± 0.02 mm^{-1} in the emergency lane and slow-traffic lane specimens, respectively. The crack surface ratio was 2.2- ± 0.2% and 3.1 ± 0.4%, in the emergency lane and slow traffic lane concrete, respectively. Both parameters indicate a greater degree of cracking of concrete taken from the slow traffic lane, by about 20% and 42%, respectively.

With the digital reconstruction of coarse aggregate distribution and the crack system as illustrated in Fig. 2, the characteristics of crack system within coarse aggregate grains in concrete was obtained. The results are provided in Table 7. Cracks in aggregates grains are by far more frequently observed in quartzite aggregate than in other aggregate, the difference is of an order of magnitude. A greater degree of cracking of aggregate grains, by about 21% and 28%, in concrete taken from the slow traffic lane, is shown by the crack length ratio and crack surface ratio, respectively. The evaluation of preexisting cracks in virgin quartzite aggregate from the quarry resulted in the crack surface ratio of 1%. Such result was quite close to cracking of all other aggregate in concrete, but cracking of quartzite in concrete was 15–18 times more intensive. Similar relationship is found for crack length ratio.

Results of evaluation of microcrack system in aggregate grains performed on SEM images are given in Table 8. The effects of concrete core localization are strong: the microcrack length and surface ratio are more than 5 times and 3 times higher for the slow traffic lane, respectively. Although these results cannot be directly compared with Table 7, because they are obtained using different methods with the resolution differing by an order of magnitude, both of them indicate substantial differences in deterioration of

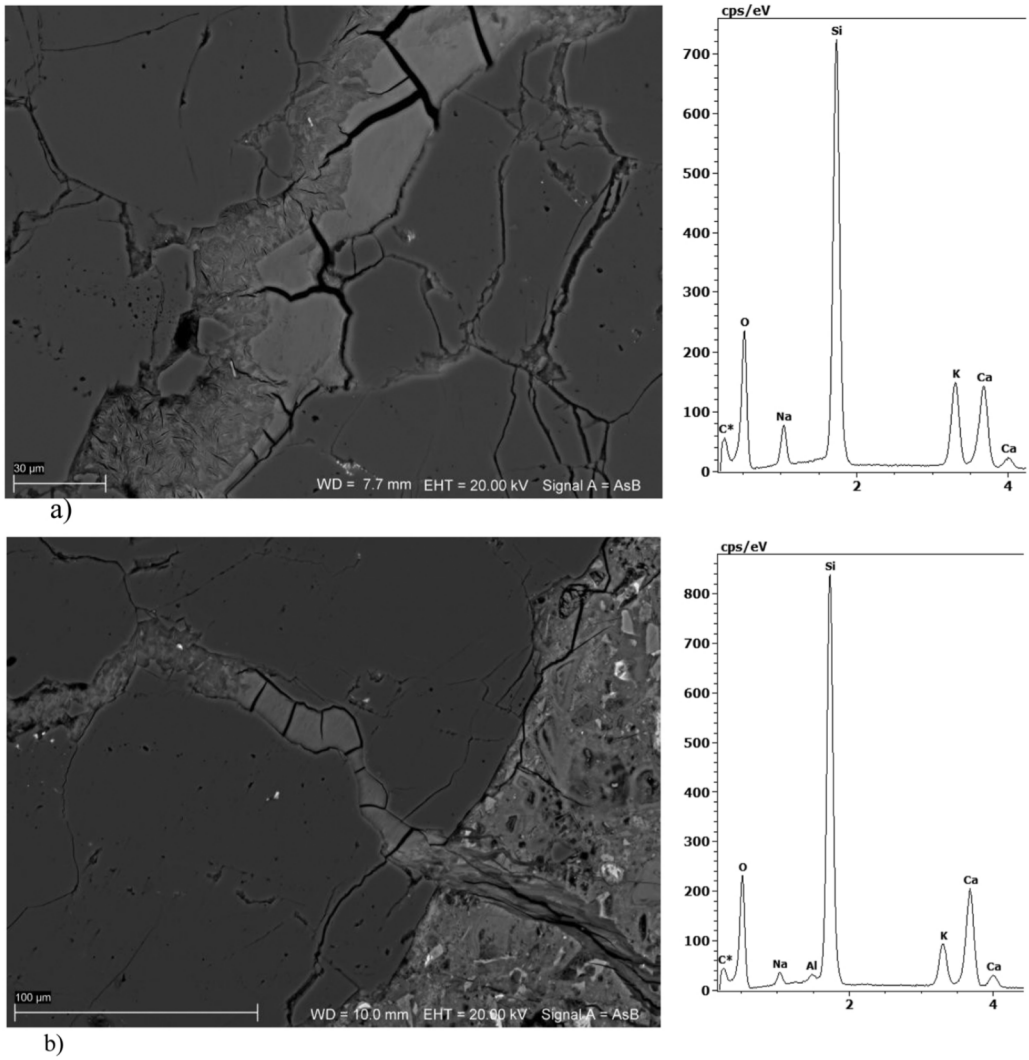

Fig. 8. EDS analysis in selected microareas within the specimen: a) 10 A, b) 10B: ASR product composition in quartzite aggregate (the potassium sodium calcium silicate).

Table 6
Results of EDS microanalysis of alkali-silica reaction products inside cracks in quartzite aggregate – the ratios of sodium, potassium and calcium to silicon, determined on polished sections of pavement concrete (the average of at least twenty five different micoareas).

Specimen No.		Na/Si	K/Si	(Na+K)/Si	Ca/Si
5B	Average	0.07	0.32	0.39	0.48
	Min	0.04	0.21	0.29	0.29
	Max	0.10	0.40	0.46	0.61
6 A	Average	0.06	0.23	0.28	0.30
	Min	0.01	0.09	0.11	0.11
	Max	0.13	0.32	0.42	0.69
7 A	Average	0.05	0.18	0.23	0.41
	Min	0.02	0.05	0.07	0.10
	Max	0.11	0.42	0.44	0.92
8 A	Average	0.06	0.18	0.24	0.60
	Min	0.01	0.03	0.04	0.18
	Max	0.21	0.45	0.57	0.93
10 A	Average	0.06	0.29	0.35	0.61
	Min	0.03	0.14	0.17	0.28
	Max	0.13	0.46	0.51	1.16
10B	Average	0.11	0.34	0.40	0.49
	Min	0.02	0.07	0.09	0.08
	Max	0.23	0.44	0.52	0.95

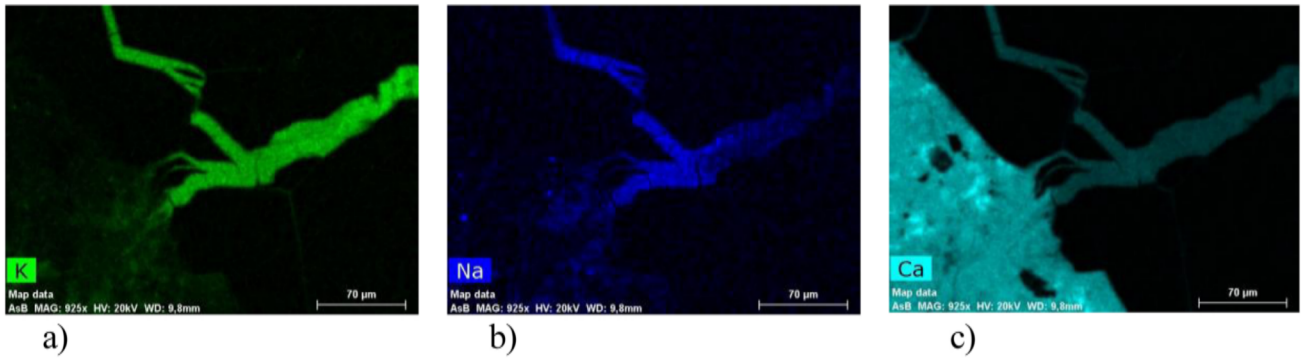

Fig. 9. Map of the atomic concentration of: a) K, b) Na and c) Ca elements in the area of cracked quartzite grain in 10 A specimen (penetration through the grain-paste boundary), scale bar 70 µm.

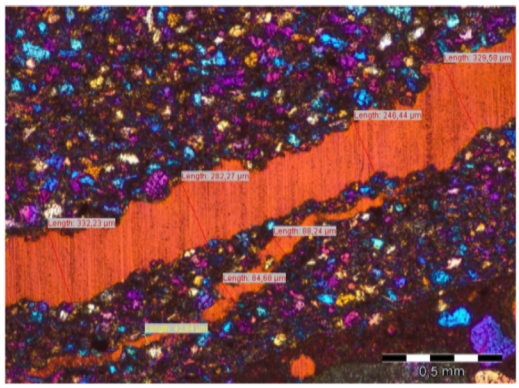

Fig. 10. Crack width in quartzite aggregate grain, 8 A; XPL_G, scale bar 0.5 mm.

Table 7
Crack system characteristics in coarse aggregate grains in concrete specimens from emergency lane and slow-traffic lane of highway pavement and in virgin quartzite aggregate.

Traffic lane	Aggregate grains	Crack length ratio[a] [mm^{-1}]		Crack surface ratio[a] [%]	
Slow-traffic	quartzite	4.03 (all grains)	6.73	11.1 (all grains)	18.5
	all other		0.47		1.5
Emergency	quartzite	3.32 (all grains)	5.70	8.7 (all grains)	14.6
	all other		0.39		1.4
None (aggregate from quarry)	quartzite	0.50		1.0	

[a] the crack length ratio and crack surface ratio are defined in respect to the cross-section area of aggregate grains > 2 mm in at least one direction.

Table 8
Microcrack system characteristics in coarse aggregate grains in concrete specimens from emergency lane and slow-traffic lane of highway pavement.

Specimen/traffic lane	Total crack length [mm]	Total crack surface area [mm^2]	Crack length ratio [mm^{-1}]	Crack surface ratio [%]
8 A/slow-traffic	1815	6.2	21.09	3.32
7 A/emergency	435	3.6	4.37	1.03

concrete in adjacent traffic lanes that are exposed to identical weather conditions but strongly differ in heavy traffic loading.

3.3. Elastic modulus and expansion of concrete specimens

The elastic properties of concrete were evaluated by measurements of the fundamental flexural resonant frequency in a Grindosonic instrument. Results presented in Table 9 were obtained on specimens from the emergency lane of pavement and also on reference specimens from trial paving section of concrete road built in 2018. The choice of the reference concrete was arbitrary- based on a similitude of designed compressive strength class (C35/45), the volume content of aggregate in concrete and a similar slip-form paving technology. A need for a reference concrete was justified due to unconventional dimensions of specimens cut from the cores (the same

Table 9
Dynamic modulus of elasticity (resonance) of concrete determined on specimens from investigated pavement section and reference trial pavement section.

Concrete specimens	Dynamic elastic modulus [GPa]	
	Average value	Standard deviation
Emergency lane[a]	17.5	3.0
Reference pavement – trial section[b]	42.8	1.6
Calculated as per fip Model Code 2010	40.8[c]	–

[a] Slow-traffic lane specimens not possible to be cut from the cracked cores
[b] Specimens of the same size cut out of cores from trial section of slip-formed pavement of C35/45 concrete with amphibolite aggregate;
[c] $40.8 = 21.5 \bullet 1.0 \bullet (40.0/10)^{(1/3)} \bullet 1.2$ – approximate prediction for 40 MPa concrete with quartzite aggregate, assuming the ratio of dynamic/static modulus of 1.2

specimen dimensions were used).

The dynamic modulus of elasticity is low and shows increased variability, thus indicating significant variation in concrete degradation. Much larger elastic modulus was obtained on reference concrete specimens, with usual scatter in the measurements. The elastic modulus of reference concrete was quite close to a predicted value according to the formula from fib Model Code [40] for concrete with a 28-day cube strength of 40 MPa. Even with such a rough comparison, a reduction of the modulus of elasticity of concrete in the investigated pavement section due to 15 years of service can be estimated to be at least 50%.

Further potential of ASR development in concrete was investigated on prismatic specimens cut out of cylindrical cores. Specimens with embedded steel studs were exposed to ASR enhancing environment – specimens were soaked in 1 M NaOH solution and kept at the temperature of 80 °C, [41,42]. The linear expansion of specimens was steadily increasing in time, reaching (the average value ± standard deviation) of 0.07 ± 0.007% after 21 days and 0.11 ± 0.009% after 28 days of storage in NaOH solution. The observed length increase is significant. That suggests there is a substantial content and availability of reactive minerals in aggregates present to sustain expansive behavior of concrete.

Surface observations of specimens after removal from NaOH solution showed a release of translucent gel-like substance at the edges of cracks in the grains of quartzite aggregate and softening of quartzite aggregate in some areas (Fig. 11a). Swelling of quartzite aggregate grains was also observed (Fig. 11b) - revealed by splinters of grain fragments from the side surfaces of concrete specimens. Softened aggregate could be punctured with a fingernail; after the test was completed, it was easy to remove the entire quartzite aggregate without disturbing the surrounding cement matrix.

3.4. Air void characteristics and rate of water absorption

Air void characteristics of pavement concrete is presented in Table 10. The total air content in hardened concrete is low, exceeding 3% in only one of three cores. Only in one of three cores, the spacing factor was not greater than 0.20 mm and the microvoid content exceeded 1.5%. Only in the case of the # 10 core specimen, the air void characteristics could be considered appropriate in terms of adequate freeze-thaw resistance [14].

Test rate of water absorption on disk specimens from cylindrical cores revealed a low water absorption rate. The initial and secondary rate of water absorption was $6.10 \pm 0.89 \cdot 10^{-4}$ mm/s$^{1/2}$ and $6.71 \pm 0.79 \cdot 10^{-4}$ mm/s$^{1/2}$, respectively (the average for 6 specimens). This is an absorption rate typical for concrete with water to cement ratio of 0.40 with Portland cement. A lack of changes in the absorption rate at longer test periods over 1 day (the secondary absorption rate) is a phenomenon characteristic of low

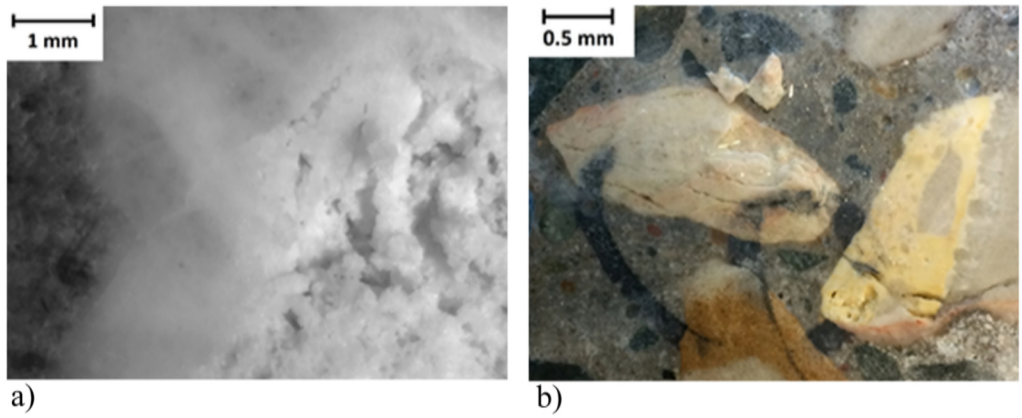

Fig. 11. View of a softened quartzite grain (a) and spalled fragments of quartzite grain (b) after 28-days storage of concrete prisms in 1 M NaOH solution at 80 °C.

Table 10
Air void characteristics in hardened concrete as per PN-EN 480–11 determined on polished section of cores from slow traffic lane of pavement.

Air void parameters	Core No.		
	5	8	10
Air content [%]	2.02	1.21	3.07
Specific surface of air voids [mm^{-1}]	24.53	29.89	30.47
Spacing factor [mm]	0.31	0.31	0.20
Microvoids content A_{300} [%]	0.72	0.60	1.69

permeability concrete. As the specimens for water absorption tests were cut from cores without delaminations or large cracks, the above results do not apply to substantially cracked pavement areas. Thus, in areas without substantial cracking, concrete does not show excessive permeability.

3.5. *Potential reactivity of quartzite aggregate*

After identification of reactive aggregate fraction, crushed quartzite aggregate from the same quarry was obtained as 2/8 and 8/16 fraction. Following the procedures ASTM C1260 [25] and AASHTO T380 [28], respective mortar and concrete specimens with quartzite aggregate and Portland cement CEM I 52.5 R (Na_2O_{eq}=0.88%) were manufactured and exposed to ASR enhancing environmental conditions. Linear expansion of specimens in time during the immersion in 1 molar NaOH solution at 80 °C (mortar) or 60 °C (concrete) is shown in Fig. 12.

An intensive expansive behavior of specimens containing quartzite aggregate is observed, both for mortar and concrete specimens. Using the relevant standard evaluation criteria for linear expansion evaluation (mortar: 0.30–0.45% at 14 days, concrete 0.121–0.240% at 56 days), both tests revealed clearly reactive behavior of quartzite aggregate.

4. Discussion

Diagnostic tests performed on concrete cores revealed a consistent set of evidence for expansive alkali-silica reaction taking place in concrete and contributing to substantial pavement cracking and spalling. The abundance of the characteristic ASR products in quartzite aggregate cracks clearly indicates the relationship between cracks in aggregate and in cement paste, and expansive alkali-silica reaction. The most common concentration ratio (Na+K)/Si and Ca/Si, known from literature for alkali-silica reaction products is about 0.20–0.35 [34] and 0.15–0.25 [35], respectively. ASR products exist in two known forms, either amorphous or crystalline [35,36,43,44]. The current investigation showed the presence of both crystalline and amorphous ASR products (Fig. 8). However, while the crystalline ASR product was found in cracks in aggregate grains, its amorphous form was present not only in the cement matrix but also in the aggregate grains, closer to their edges. A systematic differentiation of the ASR product composition depending on the place of occurrence within the microstructure was found. The ratio of alkali to silica was characterized by the typical values, while the Ca/Si ratio was greater than commonly known, however also found in the literature [34]. It is known that the composition of the ASR products changes with time [34], therefore the increase in Ca/Si ratio can be explained.

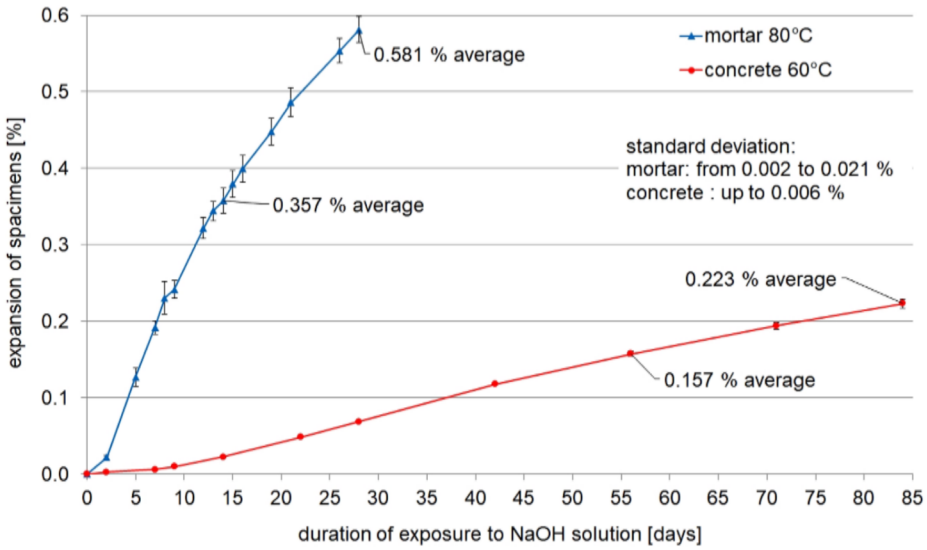

Fig. 12. Expansion of specimens containing crushed quartzite aggregate during the immersion in 1 molar NaOH solution at 80 °C (mortar, [25]) and 60 °C (concrete, [28]).

The investigated section of highway pavement was constructed using materials compliant with the then standards and technical specifications. An acceptance of quartzite aggregate was based on a simple chemical test for potential reactivity. The currently performed diagnostic tests on pavement concrete revealed that the former evaluation was erroneous because it missed the presence of micro- and cryptocrystalline quartz. Stark [45] stated that chemical methods appear to have some serious limitations to identify slowly reactive aggregates such as quartzite. An inconsistent evaluation of ASR potential of quartzite aggregate based on chemical test, in contrast to accelerated mortar bar test, was also reported by Šachlová et al. [46]. Jensen et al. [47] reported the occurrence of alkali-silica reaction in concrete containing quartzite aggregate from Thailand with the individual quartzite crystals in the size range from 10 to 50 μm, that is in accordance with the present findings.

For ASR diagnosis it is also important to determine the composition of pore solution in concrete. Unfortunately the current investigation failed to provide the conclusive data, although the pore solution extraction was attempted using a high-pressure device [48]. The specimens were too dry for meaningful measurements, and such a condition is known to be detrimental for such tests [49]. When exposed to deicing salt solution, the chemistry of the pore solution in concrete is expected to change. Heisig et al. [50] showed that during NaCl ingress the OH^- concentration of the pore solution was lowered mainly by potassium leaching and also due to the formation of Friedel's salt from ettringite. However, the silicon concentration in the pore solution was higher due the higher total alkali concentration, thus causing intensified ASR damage. Model predictions [51] show also that ASR induced expansion in concrete subjected to external alkali supply is governed by microcracking in both the aggregates and the cement paste, while the water exposure results mainly in microcracking in the aggregate.

For determination of the residual swelling potential of concrete, the method similar to Japanese short-term method was selected for the current investigation [41,42]. The criteria for judging the deleterious reactivity of aggregate in extracted concrete specimens exposed to 1 M NaOH solution at 80 °C are: the expansion of 0.1% at 3 weeks for the early-expansive aggregate (volcanic rocks) or 0.04% for the late expansive aggregate. With these criteria, considering the effect of reduced cross section and an increased absorption of NaOH solution [42], the currently determined expansion of 0.07% after 21 days is a clear indication of residual potential for late-expansive behavior of quartzite rock aggregate in concrete. Such evaluation can be treated as the ultimate degree of reactivity of aggregates with excess alkalis. For the external-alkali environment it seems more appropriate than an evaluation based on high-humidity environmental exposure. The residual swelling potential evaluation was supported by observations of exudates from cracks and spalling of quartzite grains, indicating a sufficient residual content of reactive quartz in the aggregate for further development of the expansive reaction. Due to cracking of concrete in the pavement and the usual abundant use of NaCl solution for pavement de-icing, a significant presence of sodium ions coming from the outside into concrete pore solution can be predicted. Presumably, there will be no shortage of either moisture or alkali hydroxides to sustain the reaction with the quartzite.

The observed crack system in the cores, located within the quartzite grains and at grain boundaries is clearly associated with the presence of ASR products. However, the crack system shows a regular difference between the cores taken from highly loaded pavement lane (the slow-traffic lane) and the cores from occasionally trafficked lane (the emergency lane). This implies a combined effect of fatigue loading from heavy traffic, assuming that the influence of technological factors and temperature and moisture variations would be similar for the two compared pavement lanes. According to previous studies [52–54], cracking in pavements is most often initiated due to thermally induced stresses, particularly at early ages - attributed to a high temperature during the production, and possibly also to traffic load stresses; ASR plays rather a subordinate role at this stage. If moisture and alkaline deicer solutions penetrate into the pavement through existing cracks, the development of ASR would be noticeably intensified. An evidence for this is found in the examined cores from substantially cracked section (slow-traffic) and less-cracked section (emergency).

Because of a marginal air entrainment of concrete at some locations, a possible contribution of the freeze-thaw damage to the observed crack system should be also considered. Although freeze-thaw damage occurs in cold winter season, while alkali-silica reaction develops in warm seasons, the combined damage is likely to occur [12]. When the coupled damage occurs in actual pavement, it is difficult to distinguish the extent of damage coming from each of mechanisms because the mechanisms of such interaction are not well understood. Laboratory studies confirm the aggravating effect of freeze-thaw on ASR [11]. Computer simulations for air-entrained concrete [12] show that ASR products will also fill the air voids, thus disabling their function for the frost resistance. On the other hand, the freeze-thaw created crack space may postpone the expansion due to ASR. The entrained air is thought to be still beneficial for controlling the total damage, but with less efficiency. These simulation-derived findings still need to be verified by experiments.

5. Conclusions

Performed diagnostic tests on specimens drilled from a section of highway pavement after 15 years of service revealed the following conclusions.

1. Numerous cracks in the grains of coarse quartzite aggregate and cement paste were found. Petrographic analysis revealed the abundance of reactive forms of quartz in quartzite aggregate – both microcrystalline and cryptocrystalline quartz. The estimated content of reactive quartz in aggregate was higher in cracked grains (>10%) and lower in uncracked grains (<7%).
2. Gel-like products present in cracks in quartzite aggregate, in hardened cement paste and in air voids, were composed of potassium-sodium-calcium silicate. The products inside cracks in quartzite aggregate were characterized by the average ratio of (Na+K)/Si of 0.31 and Ca/Si of 0.48. The composition was typical for alkali-silica reaction product, its variability was found correlated with the distance from reactive quartzite grains.
3. The resonance modulus of elasticity of concrete specimens was approximately 18 GPa. This corresponds to an estimated relative reduction of the elastic modulus of at least 50%.

4. Expansion of concrete specimens samples exposed to an ASR-promoting environment indicated the potential for further development of the alkali-aggregate reaction. Intensive exudations from cracks and major softening of quartzite grains was observed.
5. Potential reactivity tests performed on quartzite aggregate currently produced in the same quarry revealed strong aggregate reactivity when using standard criteria for miniature concrete prism test and accelerated mortar bar test.
6. The significant role of alkali-silica reaction in inducing cracking of pavement concrete was found due to an abundant presence of ASR products in core specimens, without exception, as well as the reactive forms of minerals in quartzite grains and confirmed potential for expansion. The role of additional destructive factors, such as the impact of heavy vehicle traffic, is suggested by higher by about 37–39% relative cracking degree in slow lane specimens compared to emergency lane specimen. In the areas of deficient air entrainment of concrete, an additional destructive factor could be the aggressive action of freezing-and thawing and de-icing agents.

Declaration of Competing Interest

The authors declare that they have no known competing financial interests or personal relationships that could have appeared to influence the work reported in this paper.

Acknowledgement

The paper has been prepared as a part of RID I-37 Project “Alkaline reactivity of domestic aggregates” financed by the National Center for Research and Development, and General Directorate for National Roads and Motorways.

References

[1] I. Fernandes, Ö. Andiç-Çakir, C. Giebson, K. Seyfarth, Mainland Europe, Turkey and Cyprus, in: Alkali-Aggregate Reaction in Concrete: A World Review, edited by Ian Sims, Alan B. Poole, CRC Press, London 2017, 321–432.
[2] C. Müller, I. Borchers, E. Eickschen, Experience with ASR test methods: advice on obtaining practical evaluation criteria for performance testing and aggregate testing, Cem. Int. 11 (3) (2013) 86–93.
[3] O. Mielich, Alkali-silica reaction (ASR) on German motorways: an overview, Otto Graf. J. 18 (2019) 197–208.
[4] J.F. Munoz, C. Balachandran, M. Beyene, T.S. Arnold, A Novel Approach for the Assessment of ASR Susceptibility of Concrete Mixtures in Airfield Pavements and Infrastructure. Report No. FHWA-HRT-21–103, Federal Highway Administration, Washington, DC, 2021; https://doi.org/10.21949/1521689.
[5] B..Fournier, M.-A. Bérubé, K.J. Folliard, M..Thomas Report on the Diagnosis, Prognosis, and Mitigation of Alkali-Silica Reaction (ASR) in Transportation Structures, FHWA, Washington, DC, 2010.
[6] B.Godart, M. de Rooij, J.G.M.Wood (eds.) Guide to Diagnosis and Appraisal of AAR Damage to Concrete in Structures. Part 1 Diagnosis (AAR 6.1), RILEM State-of-the-Art Reports, Springer 2013.
[7] S.A. Marfil, P.J. Maiza, Deteriorated pavements due to the alkali–silica reaction A petrographic study of three cases in Argentina, Cem. Concr. Res. 31 (2001) 1017–1021.
[8] A..Allard, B..Fournier, J..Bastien, B..Bissonnette, L. Sanchez, J. Duchesne, Evaluation of the degree of damage caused by alkalisilica reaction in a highway pavement: a case study, 15th International Conference on Alkali-Aggregate Reaction, Sao Paulo, 2016.
[9] E..Giannini, A.E. Snyder, T. Drimalas, Diagnosis and Prognosis of ASR in an Airfield Pavement. Revista Portuguesa de Engenharia de Estruturas. Série III. n.º 15, março 2021, 35–44.
[10] A. Frýbort, D. Všianský, J. Štulířová, J. Stryk, M. Gregerová, Variations in the composition and relations between alkali-silica gels and calcium silicate hydrates in highway concrete, Mater. Charact. 137 (2018) 91–108.
[11] R.A. Deschenes, E.R. Giannini, T. Drimalas, B. Fournier, W.M. Hale, Effects of moisture, temperature, and freezing and thawing on alkali-silica reaction, ACI Mater. J. 115 (4) (2018) 575–584.
[12] F. Gong, Y. Takahashi, I. Segawa, K. Maekawa, Mechanical properties of concrete with smeared cracking by alkali-silica reaction and freeze-thaw cycles, Cem. Concr. Compos. 111 (2020), 103623, https://doi.org/10.1016/j.cemconcomp.2020.103623.
[13] S. Góralczyk Occurence and assesment of reactive aggregates in Poland, Institute of Mechanized Construction and Rock Mining, Warsaw 2003.
[14] M.A. Glinicki, R. Jaskulski, M. Dąbrowski, Design principles and testing of internal frost resistance of concrete for road structures-critical review, Roads and Bridges - Drogi i Mosty 15 (1) (2016) 21–43, https://doi.org/10.7409/rabdim.016.002.
[15] PN-B-06714–18:1977 Kruszywa mineralne - Badania - Oznaczanie nasiąkliwości (Mineral aggregates - Testing - Determination of water absorption).
[16] PN-B-06714–46: 1992 Kruszywa mineralne - Badania - Oznaczanie potencjalnej reaktywności alkalicznej metodą szybką (Mineral aggregates - Testing - Determination of the potential alkali reactivity by the quick method).
[17] PN-B-06714–19:1978 Kruszywa mineralne - Badania - Oznaczanie mrozoodporności metodą bezpośrednią (Mineral aggregates - Testing - Determination of frost resistance by the direct method).
[18] ASTM C856–17 Standard practice for petrographic examination of hardened concrete, ASTM International, West Conshohocken, PA, 2017.
[19] RILEM AAR-1.1: 2016 Detection of potential alkali-reactivity—Part 1: Petrographic examination method.
[20] D. Jóźwiak-Niedźwiedzka, R. Jaskulski, M.A. Glinicki, Application of image analysis to identify quartz grains in heavy aggregates susceptible to ASR in radiation shielding concrete, Materials 9 (4) (2016) 224-1–14, https://doi.org/10.3390/ma9040224.
[21] ASTM C295–18, Standard guide for petrographic examination of aggregates for concrete, ASTM International, West Conshohocken, PA, 2018.
[22] ASTM C1723–16 Standard guide for examination of hardened concrete using scanning electron microscopy, ASTM International, West Conshohocken, PA, 2016.
[23] M.A. Glinicki, A. Litorowicz, Crack system evaluation in concrete elements at mesoscale, Bull. Pol. Acad. Sci. Tech. Sci. 54 (4) (2006) 371–379.
[24] ASTM C215–14 Standard test method for fundamental transverse, longitudinal, and torsional resonant frequencies of concrete specimens, ASTM International, West Conshohocken, PA, 2014.
[25] ASTM C1260 - 14 Standard test method for potential alkali reactivity of aggregates (mortar-bar method), ASTM International, West Conshohocken, PA, 2014.
[26] PN-EN 480–11:2008 Admixtures for concrete, mortar and grout. Test methods. Determination of air void characteristics in hardened concrete.
[27] ASTM C1585 Standard test method for measurement of rate of absorption of water by hydraulic-cement concretes, ASTM International, West Conshohocken, PA, 2013.
[28] AASHTO T380 Standard method of test for potential alkali reactivity of aggregates and effectiveness of ASR mitigation measures (miniature concrete prism test, MCPT), 2019.
[29] M.A. Glinicki, D. Jóźwiak-Niedźwiedzka, A. Antolik, K. Dziedzic, K. Gibas, Susceptibility of selected aggregates from sedimentary rocks to alkali-aggregate reaction, Roads and Bridges - Drogi i Mosty 18 (1) (2019) 5–24, https://doi.org/10.7409/rabdim.019.001.
[30] M.A. Glinicki, ethods of qualitative and quantitative assessment of concrete air entrainment, Cem. Wapno Beton 19/81 (6) (2014) 359–369.

[31] N. Castro, B.J. Wigum, Assessment of the potential alkali-reactivity of aggregates for concrete by image analysis petrography, Cem. Concr. Res. 42 (2012) 1635–1644, https://doi.org/10.1016/j.cemconres.2012.08.009.
[32] P. Alaejos, V. Lanza, Influence of equivalent reactive quartz content on expansion due to alkali silica reaction, Cem. Concr. Res. 42 (2012), 99-10.
[33] I. Fernandes, M.A. Ribeiro, M.A.T.M. Broekmans, I. Sims (Eds.), Petrographic Atlas: Characterisation of Aggregates Regarding Potential Reactivity to Alkalis, RILEM 2016.
[34] A. Gholizadeh-Vayghan, F. Rajabipour, The influence of alkali–silica reaction (ASR) gel composition on its hydrophilic properties and free swelling in contact with water vapour, Cem. Concr. Res. 94 (2017) 49–583.
[35] E. Boehm-Courjault, S. Barbotin, A. Leemann, K. Scrivener, Microstructure, crystallinity and composition of alkali-silica reaction products in concrete determined by transmission electron microscopy, Cem. Concr. Res. 130 (2020), https://doi.org/10.1016/j.cemconres.2020.105988.
[36] R. Dähn, A. Arakcheeva, P. Chaub, P. Pattison, G. Chapuis, D. Grolimund, E. Wieland, A. Leemann, Application of micro X-ray diffraction to investigate the reaction products formed by the alkali–silica reaction in concrete structures, Cem. Concr. Res. 79 (2016) 49–56.
[37] Z. Shi, B. Lothenbach, The role of calcium on the formation of alk ali-silica reaction products, Cem. Concr. Res. 126 (2019), 105898, https://doi.org/10.1016/j.cemconres.2019.105898.
[38] A. Leemann, Z. Shi, J. Lindgård, Characterization of amorphous and crystalline ASR products formed in concrete aggregates, Cem. Concr. Res. 137 (2020), 106190, https://doi.org/10.1016/j.cemconres.2020.106190.
[39] X. Hou, L.J. Struble, R.J. Kirkpatrick, Formation of ASR gel and the roles of C-S-H and portlandite, Cem. Concr. Res. 34 (9) (2004) 1683–1696, https://doi.org/10.1016/j.cemconres.2004.03.026.
[40] International Federation for Structural Concrete (fib—Fédération Internationale du Béton), fib Model Code for Concrete Structures, Ernst & Sohn, Berlin, 2010.
[41] V. Saouma (Ed.), Diagnosis and Prognosis of Alkali Aggregate Reactions Affected Structures – State of the art report of the RILEM Technical Committee 259-ISR, Springer International Publishing, 2021.
[42] T..Katayama, Chapter 6. Accelerated expansion test: Japan, in: V. Saouma (ed.), Diagnosis and Prognosis of Alkali Aggregate Reactions Affected Structures – State of the art report of the RILEM Technical Committee 259-ISR, Springer International Publishing, 2021, 133–162.
[43] K. Peterson, D. Gress, T. van Dam, L. Sutter, Crystallized alkali-silica gel in concrete from the late 1890s, Cem. Concr. Res. 36 (2006) 1523–1532.
[44] A. Leemann, Raman microscopy of alkali-silica reaction (ASR) products formed in concrete, Cem. Concr. Res. 102 (2017) 41–47.
[45] D. Stark, Alkali-silica reactions in concrete, in: J.F. Lamond, R.H. Pielert (Eds.), Significance of Test and Properties of Concrete and Concrete Making Materials, ASTM International, 2006, pp. 401–409.
[46] Š. Šachlová, A. Kuchaová, Z. Pertold, R. Přikryl, Microscopic and chemical characterisation of ASR induced by quartz-rich aggregates, 15th Euroseminar on Microscopy Applied to Building Materials, 16–19 June 2014, Delft, 1–10.
[47] V. Jensen, S. Sujjavanich, Alkali silica reaction in concrete foundations in Thailand. 15th Int. Conference on Alkali-Aggregates Reaction, Sao-Paulo, Brazil, 2016, no. 201.
[48] T. Kim, J. Olek, Influence of alkali-silica reaction on the chemistry of pore solutions in mortars with and without lithium ions, Proc. Int. Symp. Brittle Matrix Composites 10, Woodhead Publ., Warsaw, 2012, 11–20.
[49] G. Plusquellec, M.R. Geiker, J. Lindgård, J. Duchesne, B. Fournier, K. DeWeerdt, Determination of the pH and the free alkali metal content in the pore solution of concrete: Review and experimental comparison, Cem. Concr. Res. 96 (2017) 13–26, https://doi.org/10.1016/j.cemconres.2017.03.002.
[50] A. Heisig, L. Urbonas, R.E. Beddoe, D. Heinz, Ingress of NaCl in concrete with alkali reactive aggregate: effect on silicon solubility, Mater. Struct. 49 (2016) 4291–4303. DOI 10.1617/s11527-015-0788-y+.
[51] T. Iskhakov, C. Giebson, J.J. Timothy, H.M. Ludwig, G. Meschke, Deterioration of concrete due to ASR: experiments and multiscale modeling, Cem. Concr. Res. 149 (2021), 106575, https://doi.org/10.1016/j.cemconres.2021.106575.
[52] R. Breitenbücher, C. Sievering, Risse in Betonfahrbahndecken - Das Resultat aus Überlagerungen verschiedener, in: R. Nothnagel, H. Twelmeier (Eds.), Baustoff und Konstruktion, Springer-Verlag Berlin Heidelberg, 2013, pp. 177–188, https://doi.org/10.1007/978-3-642-29573-7_19.
[53] C. Giebson, K. Voland, H.-M. Ludwig, B. Meng, Alkali-silica reaction performance testing of concrete considering external alkalis and preexisting microcracks, Struct. Concr. (2017) 1–11, https://doi.org/10.1002/suco.201600173.
[54] R..Breitenbücher, R..Przondziono, B. Meng, E. Krütt, F..Weise, Alkali-Silica-Reaction in concrete pavements considering traffic and de-icing agents, 13th International Symposium on Concrete Roads, Berlin, June 2018.